

Solid-State Synthesis of the ZnO–Fe₃O₄ Nanocomposite: Structural and Magnetic Properties

L. E. Bykova^{a,*}, V. G. Myagkov^a, I. A. Tambasov^a, O. A. Bayukov^a, V. S. Zhigalov^a, K. P. Polyakova^a,
G. N. Bondarenko^b, I. V. Nemtsev^a, V. V. Polyakov^a, G. S. Patrin^{a,c}, and D. A. Velikanov^{a,c}

^a *Kirensky Institute of Physics, Siberian Branch of the Russian Academy of Sciences,
Akademgorodok 50–38, Krasnoyarsk, 660036 Russia*

* e-mail: lebyk@iph.krasn.ru

^b *Institute of Chemistry and Chemical Technology, Siberian Branch of the Russian Academy of Sciences,
Akademgorodok 50–24, Krasnoyarsk, 660036 Russian*

^c *Siberian Federal University, pr. Svobodnyi 79, Krasnoyarsk, 660041 Russia*

Received July 21, 2014

Abstract—The structural and magnetic properties of ZnO–Fe₃O₄ nanocomposites produced by the solid-state reaction $\text{Zn} + 3\text{Fe}_2\text{O}_3 \rightarrow \text{ZnO} + 2\text{Fe}_3\text{O}_4$ upon annealing of Zn/ α -Fe₂O₃ films under vacuum at a temperature of 450°C have been studied. Ferrimagnetic Fe₃O₄ clusters with an average grain size of 40 nm and a magnetization of ~430 emu/cm³ at room temperature, which are surrounded by a ZnO layer with a large contact surface, have been synthesized. The magnetic characteristics of the ZnO–Fe₃O₄ nanocomposite in the temperature range of 10–300 K have been presented.

DOI: 10.1134/S1063783415020079

1. INTRODUCTION

Among hybrid structures containing a ferromagnet (ferrimagnet) with a high spin polarization and a semiconductor, Fe₃O₄/ZnO heterostructures and nanocomposites have attracted attention due to the possibility of their use in optoelectronic and spintronic devices [1–12], microwave absorption [13], photocatalysis [8], cancer immunotherapy [14], and water detoxication [15]. The main requirements to such devices are high Curie temperature and high spin polarization of Fe₃O₄ and good contact between Fe₃O₄ and ZnO. Iron oxide Fe₃O₄ is a semi-metal [16, 17]; at room temperature, it has a high spin polarization, which determines the magnetoresistance—the basic characteristic of magnetic tunneling transitions [18]—and has a high Curie temperature ($T_C = 858^\circ\text{C}$) [19]. Zinc oxide ZnO is a wide-band-gap ($E_g = 3.37$ eV) semiconductor material with the exciton binding energy of 60 meV and *n*-type electronic conduction, which exhibits unique optical and electrical properties [20].

The ZnO–Fe₃O₄ magnetic nanocomposites are produced by various chemical methods [3–11]. Pulsed laser deposition and molecular beam epitaxy are the main methods of epitaxial growth of Fe₃O₄ on ZnO(001) substrates for the formation of Fe₃O₄/ZnO heterostructures [8–14]. However, there is an urgent need of new cheap and simple techniques enhancing the functional capabilities of ZnO–Fe₃O₄ magnetic nanocomposites.

In this work, we studied the structural and magnetic properties of the ZnO–Fe₃O₄ film nanocomposite produced by annealing of a Zn/Fe₂O₃ bilayer.

2. SAMPLE PREPARATION AND EXPERIMENTAL TECHNIQUE

The synthesis of ZnO–Fe₃O₄ nanocomposite films was performed by the solid-state reaction



and consisted of two stages.

(1) Preparation of Zn/ α -Fe₂O₃ bilayers, which included the following stages:

(a) thermal deposition of Fe films with a thickness of ~100 nm in a 10^{–6} Torr vacuum onto 0.18-mm-thick glass substrates;

(b) formation of α -Fe₂O₃ films as a result of oxidation of Fe layers in air at a temperature of 350°C for 10 min;

(c) thermal deposition of a Zn layer with a thickness of ~25 nm in a 10^{–6} Torr vacuum onto the α -Fe₂O₃ film surface.

To prevent the uncontrolled reaction between Zn and α -Fe₂O₃ layers, the deposition of Zn was performed at room temperature.

(2) The annealing of the synthesized Zn/ α -Fe₂O₃ samples in a 10^{–6} Torr vacuum in the temperature

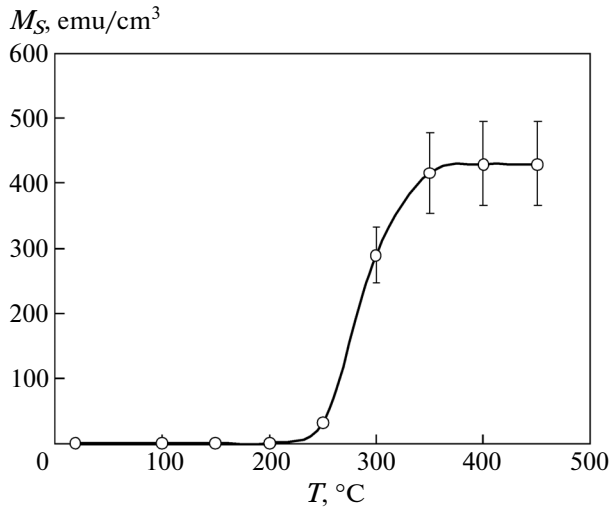


Fig. 1. Magnetization M_S of the Zn/Fe₂O₃ film as a function of the annealing temperature.

interval from 50 to 450°C with a step of 50°C and exposure at each temperature for 30 min.

The X-ray fluorescence analysis was used for determining the thickness of Zn and Fe layers. The magnetization measurements were performed on a rotating magnetometer after the annealing of the film in a 10⁻⁶ Torr vacuum by the method proposed in [21].

The temperature dependence of the resistivity of the Zn/α-Fe₂O₃ film was measured by the four-probe method with pressed contacts in a 10⁻⁶ Torr vacuum at the heating rate of ~5 K/min. The phase composition was studied by the X-ray diffraction method on a DRON-4-07 diffractometer using the CuK_α radiation (at the wavelength of 0.15418 nm).

The Mössbauer spectrum of the synthesized ZnO–Fe₃O₄ nanocomposite was measured at room temperature on an MS-1104Em spectrometer with a ⁵⁷Co(Cr) source in the constant acceleration mode. In the range of temperatures from 4 to 300 K, the saturation magnetization M_S of the ZnO–Fe₃O₄ nanocomposite films was measured on an MPMS-XL SQUID-magnetometer in a magnetic field of 500 Oe applied in the film plane and the magnetization reversal curves were measured by means of a Nano MOKE 2 magneto-optical magnetometer in a magnetic field of up to 1 kOe.

3. EXPERIMENTAL RESULTS AND DISCUSSION

The initial Zn/α-Fe₂O₃ samples represented a bilayer film system, which was confirmed by the X-ray spectrum containing only reflections from phases of Zn and α-Fe₂O₃ (not presented in the paper).

Figure 1 shows the dependence of the saturation magnetization M_S of a Zn/α-Fe₂O₃ film sample on the

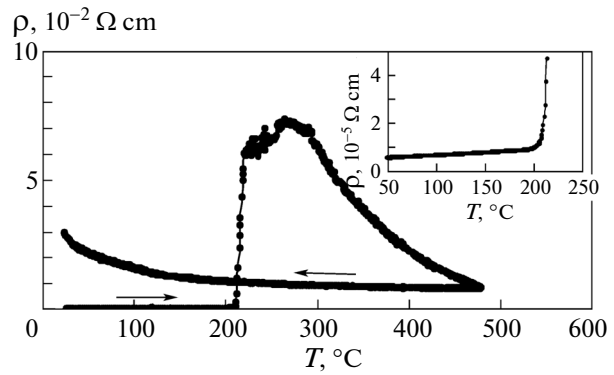


Fig. 2. Resistivity of the Zn/Fe₂O₃ film as a function of the annealing temperature.

annealing temperature. The initial Zn/α-Fe₂O₃ samples had a low magnetization of ~2 emu/cm³, which is close to the saturation magnetization of the α-Fe₂O₃ phase [22]. After annealing to the temperature of 200°C, the magnetization M_S remained unchanged. This indicates the absence of mixing and formation of compounds on the Zn/α-Fe₂O₃ interface. At the annealing temperatures above 250°C, the magnetization of M_S abruptly increased and, at 400°C, attained the maximum value, which did not vary until reaching the temperature of 450°C (Fig. 1). The increase in the magnetization M_S at temperatures above 200°C unequivocally indicates the onset of solid-state reaction (1) between Zn and α-Fe₂O₃ layers and formation of magnetic compounds. At the annealing temperature of 450°C, the reaction completely terminates.

The results of measuring the electrical resistivity ρ as a function of the temperature of annealing of Zn/α-Fe₂O₃ samples are presented in Fig. 2; they agree with the temperature measurements of the saturation magnetization M_S of these samples (Fig. 1). From Fig. 2 (inset) we see that, up to ~200°C, the resistance of the Zn/α-Fe₂O₃ film has a metallic character, which is determined by the upper zinc layer. Above ~200°C, the resistance of the film abruptly increases, which indicates fast mutual migration of Zn atoms and α-Fe₂O₃ and the onset of reaction (1). The slow increase with small oscillations up to temperatures of ~300°C reflects the unstable and nonequilibrium regime of the ZnO–Fe₃O₄ composite formation. The descending section of the temperature dependence of the resistivity up to temperatures of ~450°C, probably, is associated with post-reaction relaxation processes such as the increase in the crystal size and crystalline perfectness of grains of the ZnO–Fe₃O₄ composite.

After cooling, the dependence of the resistivity of the film has a semiconductor behavior. The dependences of the magnetization (Fig. 1) and resistivity (Fig. 2) on the annealing T temperature imply that the

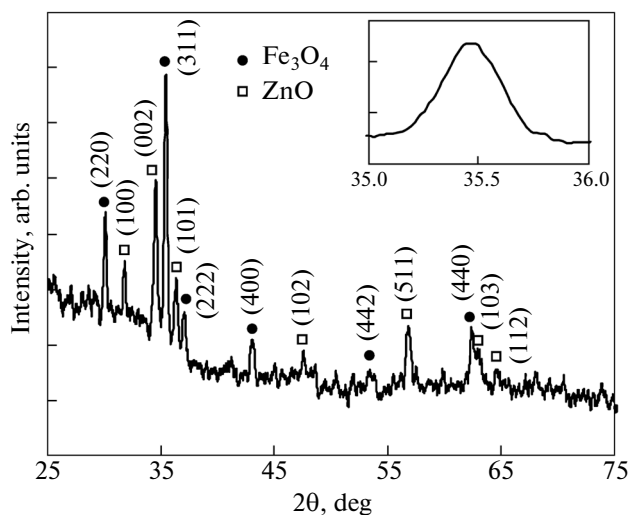


Fig. 3. X-ray diffraction pattern of the ZnO–Fe₃O₄ nanocomposite film.

temperature for the initiation of solid-state reaction (1) is $\sim 200^\circ\text{C}$.

After the annealing at 450°C , the diffraction reflections contained only peaks from polycrystalline phases of ZnO and Fe₃O₄ (Fig. 3). The Fe₃O₄ grain size was estimated from the widening of the Fe₃O₄ (311) reflections (Fig. 3, inset) by the Scherrer formula $d = k\lambda/\beta\cos\theta$, where d is the mean crystal grain size, β is the diffraction maximum width measured at half the maximum, λ is the X-ray radiation wavelength (0.15418 nm), θ is the diffraction angle corresponding to the maximum of the peak, and $k = 0.9$. The obtained calculated size of crystal grains of Fe₃O₄ was 38 ± 2 nm, which agrees well with the data obtained by a Hitachi S5500 scanning electron microscope (Fig. 4). The electron microscopy results (Fig. 4) imply that Fe₃O₄ grains of the ZnO–Fe₃O₄ composite are surrounded by a ZnO shell. The Mössbauer studies have confirmed the formation of Fe₃O₄ magnetite in Zn/ α -Fe₂O₃ films after annealing at 450°C (Fig. 5). The Mössbauer spectrum contained two sextets (see the table). The first sextet has an isomer shift with respect to α -Fe IS = 0.26 mm/s, the quadrupole splitting QS = -0.03 mm/s, and the hyperfine field $H = 488$ kOe, which corresponds to tetrahedral positions (A) of magnetite. The second sextet has IS = 0.61 mm/s, QS = -0.04 mm/s, and $H = 454$ kOe, which corresponds to iron of mixed valence: octahedral positions (B) of magnetite. It is known that, for stoichiometric magnetite, the ratio between tetrahedral and octahedral positions is 1 : 2. It follows from the table that the synthesized ZnO–Fe₃O₄ composite has a composition close to stoichiometric. No Fe-based phases beside Fe₃O₄ have been found in reaction products.

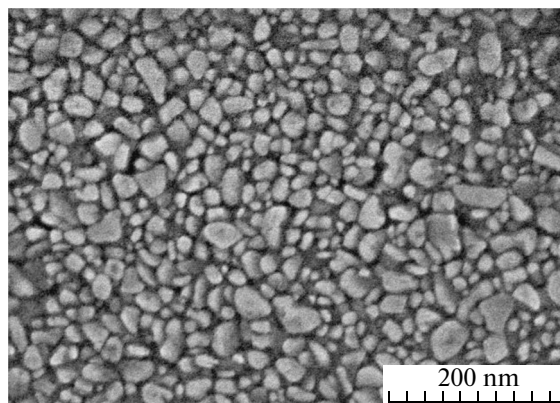


Fig. 4. Scanning electron microscopy image of the ZnO–Fe₃O₄ nanocomposite film surface.

It should be noted that the method of synthesis presented above was successfully used for producing Fe–In₂O₃ films [23], in which zinc was replaced by indium.

Figure 6 presents the temperature dependence of the magnetization of M_S of the ZnO–Fe₃O₄ nanocomposite films in a field of 500 Oe applied in the film plane. The magnetic structure of Fe₃O₄ magnetite is known well [24, 25]. Fe₃O₄ is a ferrimagnet at temperatures below $T_C = 858$ K and, as a result of the variation in the crystal structure, suffers the Verwey transition (the metal–insulator transition) at the temperature $T_V \approx 123$ K. On the curve of the temperature of magnetization (Fig. 6) near the temperature of ~ 120 K, there is an anomaly corresponding to the Verwey transition, which is also confirmed by the presence of Fe₃O₄ magnetite in synthesized samples.

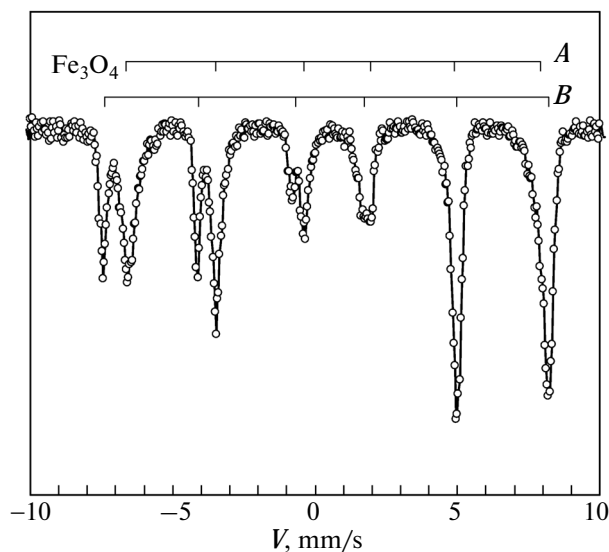


Fig. 5. Mössbauer spectrum of the ZnO–Fe₃O₄ nanocomposite film.

Mössbauer parameters of the ZnO–Fe₃O₄ nanocomposite films measured at room temperature

IS, mm/s (±0.005)	<i>H</i> , kOe (±5)	QS, mm/s (±0.02)	<i>W</i> , mm/s (±0.02)	<i>S</i> , % (±0.33)	Position
0.26	488	−0.03	0.27	0.33	Fe ³⁺ (<i>A</i>)
0.61	454	−0.04	0.36–0.57	0.67	Fe ^{2.5+} (<i>B</i>)

IS is the isomer chemical shift with respect to α -Fe, *H* is the hyperfine field, QS is the quadrupole splitting, *W* is the line width, and *S* is the population of the position.

At room temperature, the synthesized ZnO–Fe₃O₄ composite has the saturation magnetization of ~430 emu/cm³ (Fig. 1). This value exceeds the saturation magnetization of the ZnO–Fe₃O₄ composites prepared by chemical methods [5–11]. However, it is lower than the saturation magnetization of bulk samples (~480 emu/cm³), which is explained by the non-collinearity of spins on the Fe₃O₄/ZnO interface [6].

The magnetization reversal in the film plane in the range of temperatures from 4 to 300 K was measured by a Nano MOKE 2 magneto-optical magnetometer in the field of up to 1 kOe (Fig. 7). The cooling of samples was performed in two modes: in the absence of the external magnetic field (ZFC) and in a constant magnetic field (FC) of 1 kOe applied in the film plane. Figure 7 (inset) shows the ZFC curves for the magnetization reversal of films at the temperatures of 290 K (curve 1) and 90 K (curve 2). From the magnetization reversal curves, the values of the coercive force at different measuring temperatures were obtained. Figure 7 shows the temperature dependences of the coercive force for the FC (curve *a*) and ZFC (curve *b*) cooling modes. As we see, the difference in the character of temperature dependences is observed in the temperature interval 10–130 K. Moreover, the coercive force decreases with decreasing temperature in both the

cases. The temperature of 130 K is close to the Verwey transition temperature in magnetite ($T_V \approx 123$ K). The influence of the magnetic prehistory on the magnetic properties of magnetite is known and is connected with the variation in the crystalline symmetry and magnetic anisotropy in the region of the Verwey transition. The direction of uniaxial magnetocrystalline anisotropy upon cooling below the Verwey temperature in a single crystal is determined by the magnetic field applied in the direction of one of the edges of a cubic crystal [26]. In this connection, we can assume that the magnetic field has an effect on the character of the temperature dependence of the coercive force in ZnO–Fe₃O₄ composite films. At room temperature, the obtained films are magnetically isotropic. Upon cooling in a magnetic field through the Verwey point, the easy axis of magnetic anisotropy of uniaxial symmetry in a polycrystal can be any chosen direction coinciding with the direction of the applied magnetic field. Upon cooling without a magnetic field, we can expect the absence of a preferred direction of the magnetic uniaxial anisotropy. It should be noted that the sign of change in the coercive force with a decrease in

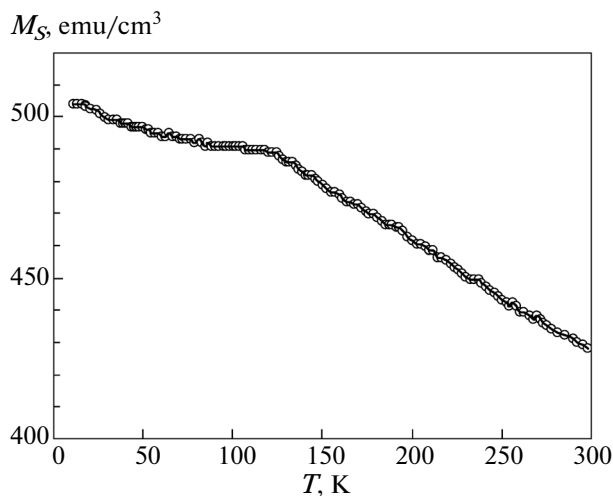


Fig. 6. Temperature dependence of the saturation magnetization M_S of the ZnO–Fe₃O₄ nanocomposite films.

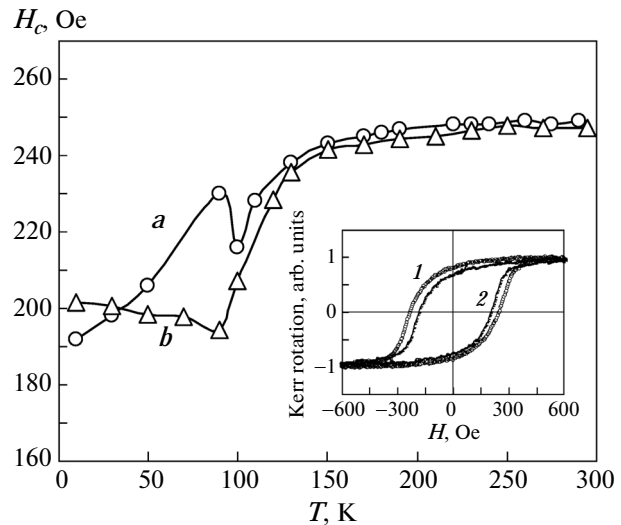


Fig. 7. Magnetization reversal curves of the ZnO–Fe₃O₄ nanocomposite films measured at temperatures of (1) 290 and (2) 90 K in the ZFC mode (shown in the inset) and temperature dependences of the coercive force measured in the FC (curve *a*) and ZFC (curve *b*) cooling modes.

temperature in both the cooling modes in our films is opposite to the sign of the variation in the coercive force of most of magnetic materials, including $\text{Fe}_3\text{O}_4/\text{ZnO}$ epitaxial heterostructures [27].

The unusual behavior of the coercive force, namely, its decrease with decreasing temperature in the obtained $\text{ZnO}-\text{Fe}_3\text{O}_4$ film composites can be caused by anomalies in the temperature dependence of the magnetic crystallographic anisotropy [6] and the influence of the composite structure of the obtained films.

4. CONCLUSIONS

The main results of our study can be summarized as follows. The $\text{ZnO}-\text{Fe}_3\text{O}_4$ ferrimagnetic composite films were prepared by solid-state reaction (1) in a layered $\text{Zn}/\text{Fe}_2\text{O}_3$ structure. The temperature for the initiation of the reaction ($\sim 200^\circ\text{C}$) was determined. The complex of the performed structural studies unambiguously indicates the formation of magnetite Fe_3O_4 and ZnO in the reaction products. The specific features were revealed in the behavior of the temperature dependences of the saturation magnetization and coercive force of the synthesized $\text{ZnO}-\text{Fe}_3\text{O}_4$ composite films near the Verwey temperature. The solid-state method can be extended by synthesizing other composite films containing ferrimagnetic Fe_3O_4 clusters embedded in metallic or more complex oxides.

REFERENCES

1. A. Roychowdhury, A. K. Mishra, S. P. Pati, and D. Das, *AIP Conf. Proc.* **1447**, 283 (2012).
2. R. Master, R. J. Choudhary, and D. M. Phase, *J. Appl. Phys.* **108**, 103909 (2010).
3. P. Zou, X. Hong, X. Chu, Y. Li, and Y. Liu, *J. Nanosci. Nanotechnol.* **10**, 1992 (2010).
4. A. Hasanpour, M. Niyafar, M. Asan, and J. Amighian, *J. Magn. Magn. Mater.* **334**, 41 (2013).
5. H. L. Liua, J. H. Wub, J. H. Minb, X. Y. Zhanga, and Y. K. Kimb, *Mater. Res. Bull.* **48**, 551 (2013).
6. A. Roychowdhury, S. P. Pati, A. K. Mishra, S. Kumar, and D. Das, *J. Phys. Chem. Solids* **74**, 811 (2013).
7. M. Machovskya, I. Kuritkaa, and Z. Kozakova, *Mater. Lett.* **86**, 136 (2012).
8. J. Xia, A. Wang, X. Liu, and Z. Su, *Appl. Surf. Sci.* **257**, 9724 (2011).
9. A. Kostopoulou, F. Tétiot, I. Tsiaoussis, M. Androuridaki, P. D. Cozzoli, and A. Lappas, *Chem. Mater.* **24**, 2722 (2012).
10. J. Cao, W. Fu, H. Yang, Q. Yu, Y. Zhang, S. Wang, H. Zhao, Y. Sui, X. Zhou, W. Zhao, Y. Leng, H. Zhao, H. Chen, and X. Qi, *Mater. Sci. Eng., B* **175**, 56 (2010).
11. J. Wan, H. Li, and K. Chen, *Mater. Chem. Phys.* **114**, 30 (2009).
12. P. Li, B. L. Guo, and H. L. Bai, *J. Appl. Phys.* **109**, 013908 (2011).
13. Z. Wang, L. Wu, J. Zhou, B. Shen, and Z. Jiang, *RSC Adv.* **3**, 3309 (2013).
14. N.-H. Cho, T.-C. Cheong, J. H. Min, J. H. Wu, S. J. Lee, D. Kim, J.-S. Yang, S. Kim, Y. K. Kim, and S.-Y. Seong, *Nat. Nanotechnol.* **6**, 675 (2011).
15. S. Singh, K. C. Barick, and D. Bahadur, *J. Mater. Chem. A* **1**, 3325 (2013).
16. Z. Zhang and S. Satpathy, *Phys. Rev. B: Condens. Matter* **44**, 13319 (1991).
17. Y. Dedkov, U. Rudiger, and G. Gutherodt, *Phys. Rev. B: Condens. Matter* **65**, 914428 (2002).
18. M. Julliere, *Phys. Lett. A* **54**, 225 (1975).
19. S. Parkin, X. Jiang, C. Kaiser, A. Panchula, K. Roche, and M. Samant, *Proc. IEEE* **91**, 661 (2003).
20. A. B. Djuricic, A. M. C. Ng, and X. Y. Chen, *Prog. Quantum Electron.* **34**, 191 (2010).
21. S. Chikazumi, *J. Appl. Phys.* **32**, S81 (1961).
22. R. Skomski and J. M. D. Coey, *Permanent Magnetism* (Institute of Physics, Bristol, United Kingdom, 1999).
23. V. G. Myagkov, I. A. Tambasov, O. A. Bayukov, V. S. Zhiagalov, L. E. Bykova, Yu. L. Mikhlin, M. N. Volochaev, and G. N. Bondarenko, *J. Alloys Compd.* **612**, 189 (2014).
24. C. G. Shull, E. O. Wollan, and W. C. Koehler, *Phys. Rev.* **84**, 912 (1951).
25. K. P. Belov, *Phys.—Usp.* **36** (5), 380 (1993).
26. J. Smit and H. P. J. Wijn, *Ferrites* (Wiley, New York, 1959; *Inostrannaya Literatura*, Moscow, 1962).
27. M. Paul, D. Kufer, A. Müller, S. Brück, E. Goering, M. Kamp, J. Verbeeck, H. Tian, G. Van Tendeloo, N. J. C. Ingle, M. Sing, and R. Claessen, *Appl. Phys. Lett.* **98**, 012512 (2011).

Translated by E. Chernokozhin